Appl. Phys. A (2000) / Digital Object Identifier (DOI) 10.1007/s003390000177

Applied Physics A
Materials
Science & Processing

Orientation dependence of ferroelectricity in pulsed-laser-deposited epitaxial bismuth-layered perovskite thin films

A. Pignolet, C. Schäfer, K.M. Satyalakshmi, C. Harnagea, D. Hesse, U. Gösele

Max-Planck-Institut für Mikrostrukturphysik, Weinberg 2, 06120 Halle/Saale, Germany
(Fax: +49-345/5511-223, E-mail: pignolet@mpi-halle.de)

Received: 5 August 1999/Accepted: 16 August 1999/Published online: 23 February 2000 – © Springer-Verlag 2000

Abstract. Thin films of bismuth-layered perovskites such as $SrBi_2Ta_2O_9$, $Bi_4Ti_3O_{12}$, and $BaBi_4Ti_4O_{15}$ with preferred orientations were grown by pulsed laser deposition on epitaxial conducting $LaNiO_3$ electrodes on single-crystalline (100) $SrTiO_3$ or on top of epitaxial buffer layers on (100) silicon. A morphology and structure investigation by X-ray diffraction analysis, scanning probe microscopy, and scanning and transmission electron microscopy showed that the films consisted of both *c*-axis-oriented regions and mixed (110)-, (100)-, and (001)-oriented regions. The regions with mixed orientation featured rectangular as well as equiaxed crystalline grains protruding out of a smooth *c*-oriented background. A closer examination revealed that the regions with mixed orientation actually consisted of a *c*-axis-oriented sublayer growing directly on the epitaxial $LaNiO_3$ electrode, on top of which the growth of either (110)-, (100)-, or (001)-oriented grains took place. Macroscopic as well as microscopic measurements of the ferroelectric properties of regions with pure *c*-orientation and of regions with mixed orientations showed a clear relationship between their ferroelectric properties and their morphology and crystallographic orientation. In the regions with mixed orientation, the films exhibited saturated ferroelectric hysteresis loops with well-defined remnant polarisation P_r and coercive field E_c. The regions having *c*-axis orientation with a smooth surface morphology in contrast exhibited a linear $P-E$ curve with no hysteretic behaviour for $SrBi_2Ta_2O_9$ and $BaBi_4Ti_4O_{15}$ and a weak ferroelectric behaviour for $Bi_4Ti_3O_{12}$. This clearly showed that the ferroelectric properties of bismuth-layered ferroelectric oxides depended on the crystalline orientation of the film and that the observed ferroelectric hysteresis loops in $SrBi_2Ta_2O_9$ and $BaBi_4Ti_4O_{15}$ films were solely due to the (100)- and (110)-oriented grains. The size of the (110)- and (100)-oriented grains being of the order of 100 nm and spontaneous polarisation having been observed and switched in a controlled manner is a demonstration that ferroelectricity can exist in structures of submicrometer size. These results might have a technological impact due to the relevance of bismuth-layered ferroelectric oxides for the fabrication of non-volatile FeRAM memories.

PACS: 68.55-a; 77.80-e; 81.15.Fg

Ferroelectric thin films are a topic of current research both under applied and fundamental aspects [1–3]. Thin films of Pb(Zr, Ti)O_3 (PZT) and $SrBi_2Ta_2O_9$ (SBT) are already in use in commercial products, and SBT thin films are particularly promising as the functional elements of ferroelectric random access memories (FeRAMs) [1, 4, 5]. SBT films are advantageous over PZT films in that they do not suffer from fatigue [6, 7], whereas PZT films show considerable fatigue if used together with metallic electrodes [8, 9]. This advantage of SBT films is a consequence of the unique crystal structure of the class of materials SBT belongs to: the bismuth-layered perovskites (also called Aurivillius phases). The unit cell of the lattice of this type of compounds consists of perovskite blocks sandwiched between Bi_2O_2 layers [10–12]. The low fatigue and its relation to the crystal structure has made thin films of the Aurivillius-type ferroelectric bismuth-layered perovskites a most interesting object of investigation during recent years [5, 6, 13–28].

The ferroelectric films so far used for storage purposes in integrated solid-state memories are entirely polycrystalline in nature, i.e. they are characterised by a random distribution of grain orientations. The consequences of this random orientation distribution for the ferroelectric properties are rather well understood in the case of PZT, the crystal lattice of which is almost cubic. PZT can thus be considered fairly isotropic, which facilitates the quantitative discussion of the properties of polycrystalline PZT films [29]. In contrast, SBT has an orthorhombic crystal lattice and is characterised by a strong anisotropy of its crystal structure and thus also its ferroelectric properties. The consequences of this strong anisotropy for the properties of thin SBT films are, however, not yet well understood [24, 27, 28, 30].

Studies of crystal orientation and structure–property relationships of Aurivillius-type ferroelectric thin films are, however, also important under fundamental aspects. Early work reported the direction of the spontaneous polarisation in the Aurivillius-type compounds to be in the (*a*-*b*) plane [31]. Later on Cummins and Cross, and Aurivillius and Fang found that the spontaneous polarisation of $Bi_4Ti_3O_{12}$ and $Ba_2Bi_4Ti_5O_{18}$ has at least a measurable component in the *c* direction [11, 13].

The Aurivillius compounds are described by the general formula $(Bi_2O_2)^{2+}(A_{n-1}B_nO_{3n+1})^{2-}$, where n is the number of oxygen octahedra between the Bi_2O_2 layers and is sometimes called the Aurivillius parameter. The direction of the spontaneous polarisation in the bismuth-layered compounds has been reported to depend on the number $n-1$ of perovskite blocks between the Bi_2O_2 layers, and on whether it is even or odd [28, 32, 33]. Recently, artificial superlattices of bismuth-based ferroelectric oxides with $n = 1$ to 3 perovskite layers sandwiched between Bi_2O_2 layers and with the c axis normal to the substrate were grown by Tabata et al. They reported ferroelectric hysteresis loops for $n = 1$ or 3 whereas superlattices with $n = 2$ showed a linear $P-E$ curve. Tabata et al. therefore claim that for even n the vector of the spontaneous polarisation is completely within the *a*-*b* plane, while a small component of the spontaneous polarisation is present along the c axis for odd n [32, 33].

Independent experimental confirmation of this observation is highly desirable, if the properties of thin films of SBT and other bismuth-layered compounds are to be quantitatively understood. However, SBT thin films with a uniform orientation different from the (001)-orientation (from the '*c*-orientation') have to our knowledge been prepared only once [21]. In that work the ferroelectric properties were not measured, because the films had been grown on a non-conducting substrate. More detailed studies of structure, morphology, and orientation of SBT thin films, as well as the impact of the latter on the ferroelectric properties, are thus required.

To contribute to a better understanding of the above problems and to study structure–property relationships of Aurivillius-type ferroelectric thin films, we performed a comparative study of crystal orientation and orientation-dependent ferroelectric properties of well-oriented thin films of three different Aurivillius-type compounds, viz $SrBi_2Ta_2O_9$ (SBT, $n = 2$), $Bi_4Ti_3O_{12}$ (BiT, $n = 3$), and $BaBi_4Ti_4O_{15}$ (BBiT, $n = 4$). The films were grown by pulsed laser deposition (PLD) on epitaxial conducting $LaNiO_3$ electrodes [24, 26, 27, 34]. Structure and morphology of the films were studied by X-ray diffraction (XRD), scanning electron microscopy (SEM), scanning force microscopy (SFM), and plan-view and cross-sectional transmission electron microscopy (TEM), whereas the ferroelectric properties were determined both by macroscopic measurements and at the submicroscopic level by SFM in the piezoresponse mode [35, 36].

1 Experimental procedures

Ferroelectric thin films of $Bi_4Ti_3O_{12}$ (BiT), $SrBi_2Ta_2O_9$ (SBT), and $BaBi_4Ti_4O_{15}$ (BBiT) were epitaxially deposited by pulsed laser deposition (PLD) onto epitaxial layers of electrically conductive $LaNiO_3$ (LNO). The epitaxial LNO layers served both as template favouring the epitaxial growth of the ferroelectric films and as bottom electrodes for their subsequent electrical characterisation. The conductive LNO epitaxial layers were grown either on top of (100)-oriented $SrTiO_3$ single crystals or on top of (100)-oriented single-crystalline silicon substrates previously coated with a stack of epitaxial CeO_2 and YSZ buffer layers. YSZ stands for yttria-stabilised zirconia, i.e. ZrO_2 stabilized in its cubic phase by means of about 10 mol % Y_2O_3. The CeO_2/YSZ bilayer serves as a template to promote the epitaxial growth of the LNO electrode layer on Si(100), which in turn promotes the epitaxial growth of the bismuth-layered perovskite film [26, 27, 37].

All the films and layers were grown by PLD employing a KrF excimer laser ($\lambda = 248$ nm) at a laser repetition rate of 5 or 10 Hz. The large-area pulsed laser deposition system, as well as the rocking-target and off-axis methods used to grow epitaxial BiT, SBT, and BBiT films and to produce SBT/LNO/CeO_2/YSZ and BBiT/LNO/CeO_2/YSZ heterostructures [24, 26, 27], as well as the details of PLD of epitaxial LNO thin films and their properties [38], have been described earlier. The depositions of all the films were performed in pure oxygen atmosphere in a continuous sequence without breaking the controlled atmosphere conditions. The films were grown on substrates heated at high temperatures estimated to lie between 675 °C and 685 °C for YSZ and between 650 °C and 670 °C for the other materials. The substrate temperature was computer-controlled via a thermocouple located inside the heater. The set-temperature and temperature displayed are therefore higher than the true substrate temperature. In order to assess this difference, the actual temperature of the substrate was directly measured under the various conditions used for film deposition attaching thermocouples to several places on the substrate on a *non-rotating* substrate. At a set-temperature of 800 °C, the measured substrate temperatures were indeed smaller by about 130 °C to 150 °C than the nominal set-temperature. These measured temperatures were used as an estimation of the true substrate temperature in the actual *rotating* substrate configuration. After the deposition of the bismuth-layered perovskite film the epitaxial heterostructure was slowly cooled down to room temperature in 13.3 Pa of pure oxygen. The deposition parameters used as well as the typical thicknesses obtained for the different materials deposited, i.e.YSZ, CeO_2, LNO, $Bi_4Ti_3O_{12}$, $SrBi_2Ta_2O_9$, and $BaBi_4Ti_4O_{15}$, are summarised in Table 1.

The structure of the films was studied by X-ray diffraction (XRD) using a Philips X'Pert MRD four-circle diffractometer and plan-view and cross-section transmission electron microscopy (TEM). The film morphology was probed by scanning electron microscopy (SEM) and scanning force microscopy (SFM). Macroscopic ferroelectric measurements were carried out on planar capacitor structures employing a RT66A ferroelectric tester and a mercury probe. The spatial distribution of the ferroelectric properties, the domain

Table 1. Summary of the deposition conditions used for the growth of epitaxial YSZ, CeO_2, $LaNiO_3$ (LNO), $Bi_4Ti_3O_{12}$ (BiT), $SrBi_2Ta_2O_9$ (SBT), and $BaBi_4Ti_4O_{15}$ (BBiT) films

Deposition parameters	YSZ	CeO_2	LNO	BiT	SBT	BBiT
Repetition rate /Hz	10	10	5	10	10	10
Pulse energy /mJ	450	350	350	350	350	350
Energy density /J/cm^2 (on the target)	3	2.7	2.7	2.7	2.7	2.7
Heater temperature /°C	820	800	800	800	800	800
Substrate temperature /°C (estimated)	680	665	655	665	665	665
Oxygen pressure ×7.5/Pa	10^{-2}	100	300	100	100	100
Film thickness /nm	≈ 50	≈ 20	≈ 50	≈ 400	≈ 150	≈ 300

structure and the local hysteresis loops were investigated at the sub-microscopic level using piezoresponse scanning force microscopy (SFM). The experimental set-up was described elsewhere [35, 36] and was very similar to that reported by other authors [39, 40]. Briefly, for the piezoresponse investigations reported here, a Dimension 5000 scanning probe microscope from Digital Instruments equipped with a highly doped silicon conductive tip-cantilever assembly was used. A small ac-testing signal with a frequency of 14.2 kHz and an amplitude smaller than the coercive voltage of the film under test (typically 2–3 V) was applied between the conductive tip and the bottom electrode of the sample. The mechanical oscillations of the sample surface induced by the ac field, via the converse piezoelectric effect, were transmitted to the tip and were extracted from the global deflection signal using a lock-in technique (EG&G lock-in amplifier, model 7620). The topographic image and the domain structure image were simultaneously displayed by monitoring both the usual deflection signal and the first harmonic of the small signal induced by the ac-testing voltage (referred to as the piezoresponse signal in the following). Local piezoelectric hysteresis loops were acquired by superimposing a dc-bias voltage to the ac signal. Note that each point of the hysteresis loops was taken in *zero field* conditions after having applied a poling voltage of the desired amplitude for a duration of 100 ms, then suppressing the bias voltage and waiting for 2 s before finally measuring the piezoresponse. The use of this procedure avoided severe electrostatic interactions between cantilever/tip and bottom electrode. However, only the remnant piezoelectric coefficient was measured as a function of the voltage of the poling dc-pulse.

2 Results and discussion

2.1 Thickness and composition uniformity

The spatial thickness uniformity obtained was investigated by profilometry, ex-situ spectroscopic ellipsometry, or constant-angle reflectance interference spectroscopy (CARIS) and was locally confirmed by cross-sectional SEM. For films deposited on large areas the relative thickness variation of the whole heterostructure was strongly depending on the materials, but smaller than 15% of the average thickness over entire 3-inch wafers in the worst case. The thickness uniformity was correspondingly better for films grown on smaller size substrates, thickness variations being almost negligible for heterostructures deposited on 1 cm × 1 cm size substrates. The chemical composition of the deposited films controlled by energy-dispersive X-ray spectroscopy (EDX) and Rutherford backscattering spectroscopy (RBS) was also very good, even across the whole area of a substrate 3 inch in diameter. Both the spatial thickness and compositional uniformities were described in detail earlier and were reported elsewhere [26].

2.2 Structure and morphology

All the bismuth-layered thin films, i.e. BiT, SBT, and BBiT in this study, deposited on (100)-oriented epitaxial LNO electrodes on STO single-crystalline substrates or on top of an epitaxial buffer layer stack on single-crystalline silicon showed mainly *c*-oriented growth. The epitaxial nature of the films composing the heterostructures was shown by establishing both their good out-of-plane and in-plane orientations. X-ray diffraction (XRD) $\theta - 2\theta$ scans showed overwhelmingly $(00l)$ peaks. Figure 1a shows the X-ray spectrum in the $\theta - 2\theta$ Bragg–Brentano geometry for an epitaxial SBT film on an epitaxial $LNO/CeO_2/YSZ/Si(100)$ heterostructure. The spectrum displays only SBT $(00l)$ peaks besides the $(h00)$ peaks of the epitaxial electrode and buffer layers clearly demonstrating the good out-of-plane orientation of the SBT film. The in-plane orientation was verified by means of X-ray Φ-scans. Figure 1b shows a Φ-scan for the (208) peak ($2\Theta = 43.69°$) of the same film as in Fig. 1a. It exhibited four well-resolved peaks separated by 90° revealing a good in-plane orientation as well as the pseudo-tetragonal character of the crystallographic unit cell. Having a good out-of-plane and a good in-plane orientation, the good epitaxy of the SBT films of Fig. 1 is established. The epitaxial nature of the different layers forming the various heterostructures presented and discussed in this study was verified and was equivalent to that of the SBT films of Fig. 1. More detailed XRD texture

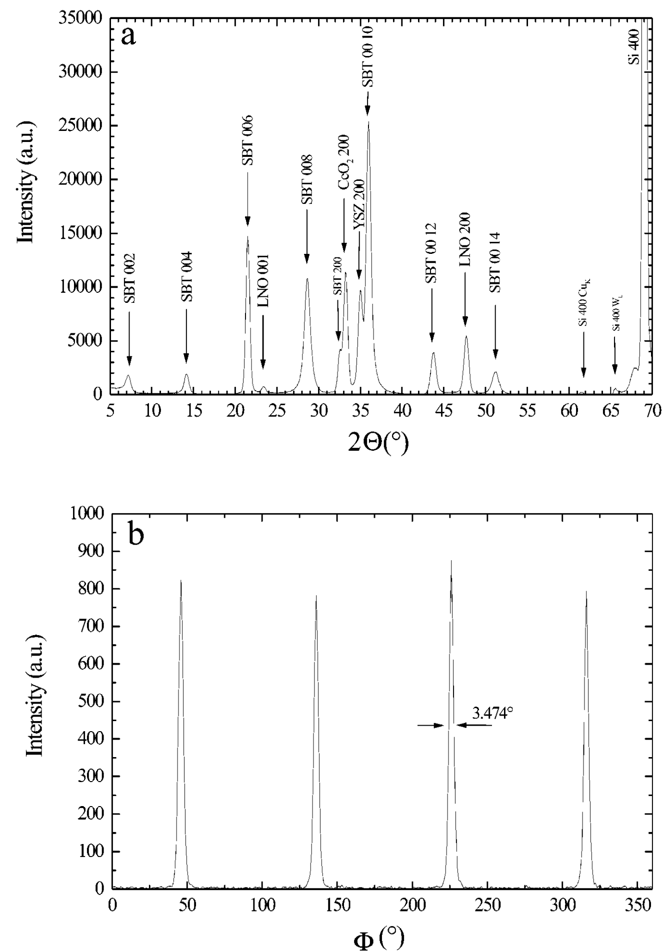

Fig. 1. **a** X-ray $\Theta - 2\Theta$-scan of a SBT film deposited onto an epitaxial LNO electrode layer on an epitaxial CeO_2/YSZ buffer layer stack on a Si(100) substrate. The spectrum displays only SBT $(00l)$ peaks besides the $(h00)$ peaks of the epitaxial electrode and buffer layers and clearly shows that the film has a good out-of-plane orientation. **b** X-ray Φ-scan for the (208) peak ($2\Theta = 43.69$) of the same film as in **a** demonstrating a good in-plane orientation, and revealing together with (**a**) the good epitaxial character of the SBT film

analysis showed, however, regions with a small film fraction having $(110)_{orth}$ and $(100)_{orth}$ orientations[1] beside the mostly (001)-oriented (i.e. *c*-oriented) film. It will be shown in the following that this observation is fully consistent with the SEM, SFM, and TEM investigations.

The morphology of the films were observed by means of SEM and SFM. Both SEM and SFM investigations revealed the same surface morphology of the epitaxial bismuth-layered films: the film exhibited rectangular as well as equiaxed grains protruding out of a flat background. Depending on the materials deposited and on the deposition conditions the density of these protruding grains differed. Although the thickness and composition were uniform across the whole samples (see above), the surface morphology and the film microstructure was not uniform across the sample area. Even for substrates of 10×10 mm, BiT, SBT, and BBiT films had regions of several mm^2 having a smooth surface and regions of several mm^2 with equiaxed and rectangular grains protruding out of the smooth background. This difference in the film morphology across the substrate is very probably due to a thermal gradient across the substrate during the film deposition, but the exact mechanism responsible for the non-uniformity of the microstructure is still under investigation. Figure 2 shows a scanning force microscopy topographic image of a region of an epitaxial SBT film with mixed orientation which exhibited a typical surface morphology. The equiaxed grains are protruding about 50 nm out of the flat surface, whereas the rectangular grains are protruding out only 20 to 30 nm. The rectangular grains are oriented with their long axis along two mutually perpendicular directions, and a similar preferred in-plane orientation seems to exist for the equiaxed grains as well (Fig. 2). SFM images of the regions without the rectangular-shaped crystallites (not shown here) displayed a highly smooth surface morphology with a root mean square (RMS) surface roughness of 2.5 nm over areas of about 2.5×2.5 µm. All these features were observed in SBT, BiT, and BBiT epitaxial films on both STO and Si-based substrates.

TEM cross-section (XTEM) images were taken from regions where a high density of rectangular-shaped and equiaxed protruding crystallites were observed by SEM and SFM. The XTEM images (Fig. 3) clearly confirmed the very flat nature of the background and the protruding character of the grains. A closer examination revealed that the regions with mixed orientation actually existed in most of the cases of two sublayers (cf. below). Higher resolution XTEM pictures of the same epitaxial SBT film as in Fig. 2b (not shown here) also exhibited periodic fringes with a spacing of 12.5 Å, corresponding to the distance between two Bi_2O_2 planes in the SBT crystal structure. These fringes were running parallel to the surface in the matrix indicating that the crystallographic *c* axis is normal to the surface. The fringes corresponding to the Bi_2O_2 planes were running perpendicular to the surface in the embedded grains [28]. Together with the presence of a fraction of SBT with (110)- and (100)-orientation inferred from the detailed analysis of the XRD

[1] Please note that the bismuth-layered perovskites have been described in the published literature either using a pseudo-tetragonal unit cell or using a unit cell with the actual orthorhombic symmetry. In all generality the "tetr." and "orth." subscripts should indicate whether the pseudo-tetragonal or the orthorhombic description, and indexation, is used. However, in the following only the orthorhombic description, corresponding to the actual symmetry, will be used, and the subscript "orth." will be omitted.

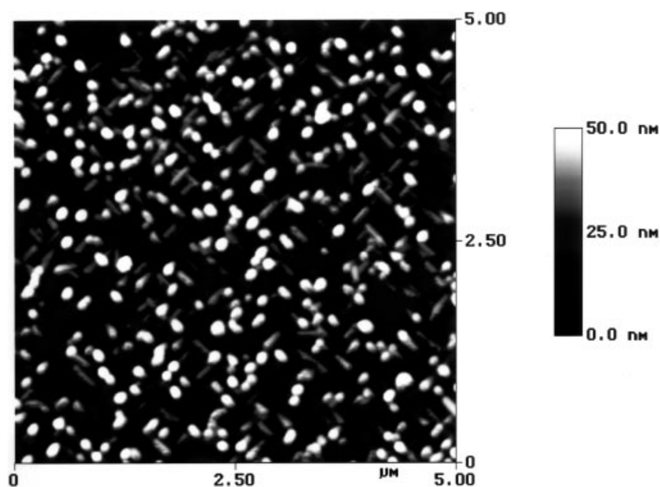

Fig. 2. Scanning force microscopy topographic image of an epitaxial SBT film showing rectangular and spherical grains protruding out of a flat background. The rectangular grains are oriented with their long axes along two mutually perpendicular directions

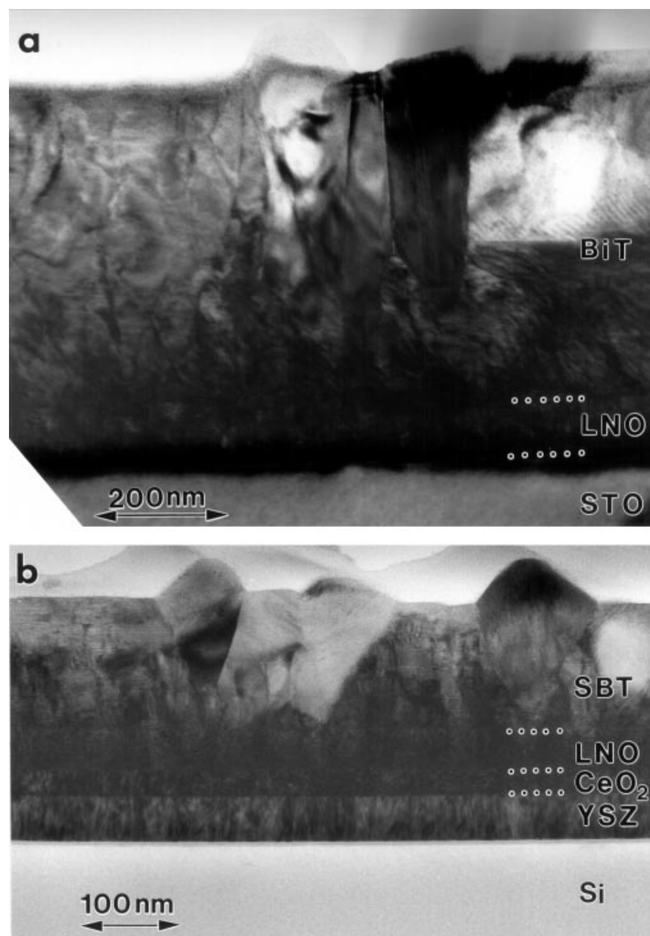

Fig. 3a,b. Cross-section TEM images of a BiT film on top of an epitaxial LNO electrode on a $SrTiO_3$ single crystalline substrate (**a**), and a SBT film deposited onto an epitaxial LNO film on an epitaxial CeO_2/YSZ buffer layer stack on a Si(100) single crystalline substrate (**b**). Both films exhibit grains about 100 nm in size protruding out of a flat background

data, this implied that the crystallographic c axis of SBT in the grains was lying parallel to the surface in the plane of the figure. A more careful analysis of the XTEM images, together with the surface morphology observed by SEM and SFM gave evidence that some grains had their c axis parallel to the surface but normal to the plane of the figure. Most of these deductions have already been confirmed by taking selected-area electron diffraction (SAED) patterns of the lower and upper sublayers and of the embedded grains (not shown here). It clearly showed that the lower layer, growing directly on the epitaxial $LaNiO_3$ electrode, was exclusively c axis oriented. On top of the c-oriented sublayer the growth of (110)- and (100)-oriented protruding grains took place, giving rise to a completely c-oriented matrix with a flat free surface with embedded grains protruding out of the surface [28]. As XTEM images of BiT/LNO/STO and of BBiT/LNO/STO [24] were showing the same features (a complete analysis of all the images is under process), it was concluded that these features are common to all our bismuth-layered epitaxial films.

Plan-view TEM images were also taken in order to determine the epitaxy relationships existing between the embedded grains having different orientations and the underlying epitaxial layers as well as their orientations relative to the single crystalline substrate. Figure 4b shows a plan-view TEM image of the same BiT film as in Fig. 3a. The image shows equiaxed "square" grains (labelled "A" and "B" in Fig. 4b) and rectangular-shaped grains (labelled "C" and "D") embedded into the c-oriented BiT film matrix. This morphology clearly reflects the one of the SFM image of Fig. 2 and is consistent with the cross-section TEM micrograph of Fig. 3a. It can be noticed that both the "square" and the "rectangular" grains are single crystalline. The diffraction patterns (a), (c), and (d) were evaluated in detail: The diffraction pattern (a), corresponding to the left part of the image, shows (i) the strong square pattern of the reflections from the $LaNiO_3(001)$ electrode layer, (ii) a weaker square pattern from the c-oriented BiT(001) film matrix, (iii) the rows of $(00l)$ reflections running from top left to bottom right corresponding to the (110)-oriented rectangular grain "C" on the left, and (iv) the two mutually perpendicular rows of $(00l)$ reflections corresponding to the (100)-oriented square grains "A" and "B" in the middle. The diffraction patterns (c) and (d), taken with the smallest selected-area diaphragm and reduced in scale by a factor of two with respect to (a), show the selected-area electron diffraction (SAED) patterns of the (100)-oriented square grain "A" and the (110)-oriented rectangular grain "D", respectively.

From a detailed analysis of these SAED patterns, the following conclusions were drawn. The $LaNiO_3$ electrode layer (LNO), if considered as pseudo-cubic[2], has the following cube-to-cube orientation relationship with respect to the $SrTiO_3$ substrate (STO):

$$(001)\mathrm{LNO} \,||\, (001)\mathrm{STO}\,; \quad [100]\mathrm{LNO} \,||\, [100]\mathrm{STO}\,. \qquad (1)$$

The c-oriented BiT film matrix ("MBiT") obeys the following orientation with respect to the $SrTiO_3$ substrate:

$$(001)\mathrm{MBiT} \,||\, (001)\mathrm{STO}\,; \quad [100]\mathrm{MBiT} \,||\, [110]\mathrm{STO}\,. \qquad (2)$$

Embedded into this matrix are grains of two different orientations, each of them existing with two mutually perpendicular azimuthal orientations. The more or less square-shaped BiT grains ("SQBiT") (for example, "A" and "B" in Fig. 4b), which in the SFM images show up as round-shaped ("spherical") grains, obey the following orientation relationships with respect to the STO substrate and the c-oriented BiT film matrix:

$$(100)\mathrm{SQBiT} \,||\, (001)\mathrm{STO} \,||\, (001)\mathrm{MBiT}; \quad [001]\mathrm{SQBiT} \,||\, [110]\mathrm{STO} \,||\, [100]\mathrm{MBiT}; \qquad (3a)$$

$$(100)\mathrm{SQBiT} \,||\, (001)\mathrm{STO} \,||\, (001)\mathrm{MBiT}; \quad [001]\mathrm{SQBiT} \,||\, [1\bar{1}0]\mathrm{STO} \,||\, [010]\mathrm{MBiT}\,. \qquad (3b)$$

The rectangular-shaped grains ("RGBiT") (for example, "C" and "D" in Fig. 4b), which in SFM images also show up with rectangular shape, obey the following orientation relationships with respect to the STO substrate and the c-oriented BiT film matrix:

$$(110)\mathrm{RGBiT} \,||\, (001)\mathrm{STO} \,||\, (001)\mathrm{MBiT}; \quad [001]\mathrm{RGBiT} \,||\, [100]\mathrm{STO} \,||\, [110]\mathrm{MBiT}; \qquad (4a)$$

$$(110)\mathrm{RGBiT} \,||\, (001)\mathrm{STO} \,||\, (001)\mathrm{MBiT}; \quad [001]\mathrm{RGBiT} \,||\, [010]\mathrm{STO} \,||\, [1\bar{1}0]\mathrm{MBiT}\,. \qquad (4b)$$

[2] Although almost cubic, $LaNiO_3$ has actually a rhombohedral symmetry. Both cubic and rhombohedral description and indexation of $LaNiO_3$ may therefore be found in the literature.

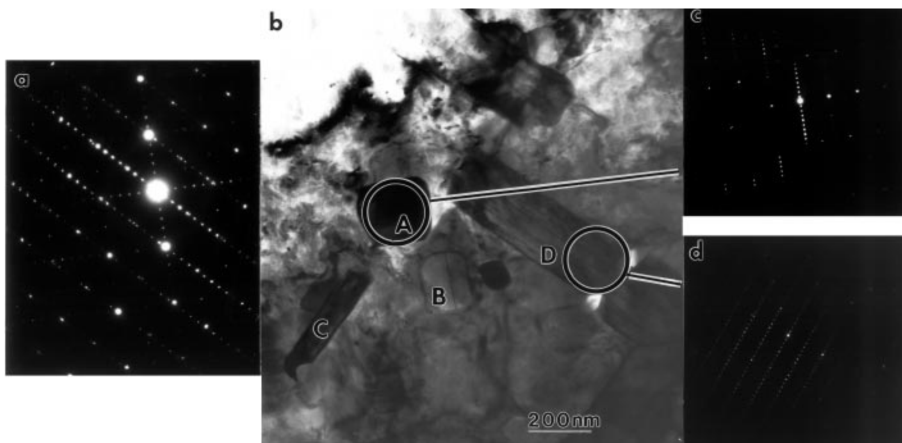

Fig. 4a–d. Plan-view TEM image (**b**) of the same BiT film as in Fig. 3a. The image shows (100)-oriented square grains ("A", "B") and (110)-oriented rectangular shaped grains ("C", "D") within a flat (001)-oriented film matrix. This morphology corresponds to that of the SFM image of Fig. 2. Details of the selected-area diffraction patterns (**a**), (**c**), and (**d**) are explained in the text. Note that (**c**) and (**d**) are reduced by a factor of two with respect to (**a**)

It can be noted that XRD, SEM, SFM, cross-section and plan-view TEM results, including the epitaxy relationships given above, are fully consistent with each other, giving them a high degree of credibility and reliability.

2.3 *Ferroelectric properties*

Layer-structured ferroelectric oxides exhibit a high degree of anisotropy in their electrical properties due to their crystal structure. For instance a high dielectric constant in the *a-b* plane and a comparatively low dielectric constant along the *c* axis have been observed in BBiT single crystals [30]. As mentioned in the introduction there is a belief that bismuth-layer-structured ferroelectric oxides with an even Aurivillius parameter *n* exhibit absolutely no spontaneous polarisation along the *c* axis whereas those with odd *n* do exhibit a small but non-zero spontaneous polarisation along the *c* axis [32, 33]. Spontaneous polarisation has indeed been measured and reported for *c*-axis-oriented BiT ($n = 3$) films [6], supporting the second part of the statement. On the other hand, some evidence to support the first part of the statement was presented by Desu et al. [41], who reported an orientation dependence of the ferroelectric properties of $SrBi_2Ta_2O_9$ (SBT) ($n = 2$) thin films grown on Pt electrodes, observing a decrease in polarisation and coercive field values with an increase in the degree of *c*-axis orientation. The experimental evidence reported by Tabata et al. [32, 33] remained however the most convincing confirmation to date. The results reported in the following sections are a further and definitive confirmation that the bismuth-layered perovskites with even Aurivillius parameter *n* have no spontaneous polarisation along their crystallographic *c*-axis, at least for epitaxial films of SBT ($n = 2$) and BBiT ($n = 4$).

2.3.1 Macroscopic ferroelectric hysteresis. As described above, the BiT, SBT, and BBiT films had regions of several mm^2 having only *c*-axis-oriented grains with a smooth surface, and regions of several mm^2 regions with (110)- and (100)-oriented crystallites embedded in the *c*-oriented film. The macroscopic ferroelectric characteristics of the epitaxial bismuth-layered films were measured using the underlying conductive epitaxial LNO layers as bottom electrodes. Ferroelectric hysteresis measurements were carried out on the bismuth-layered perovskite films, separately accessing different regions showing different morphologies by using a Hg probe with a contact area of $0.08\,mm^2$. Figure 5 shows typical ferroelectric hysteresis loops of a SBT film in a region with a high density of protruding (110)- and (100)-oriented crystallites, rectangular shaped and equiaxed, respectively, dispersed in a flat *c*-oriented background, and in a region almost purely *c*-oriented, respectively. It can be seen that also the ferroelectric properties of epitaxial SBT films are strongly related to their microstructure. The ferroelectric properties of regions of mixed orientation are weaker than for a polycrystalline film [17, 41] but the loop is saturated, the remnant polarisation $P_r \approx 1\,\mu C/cm^2$ and the switching voltage smaller than 1 V are still suitable for applications. In the region almost purely *c*-oriented, almost no hysteresis loop is observed, as is the case of completely *c*-oriented BBiT reported earlier [24]. The important result is therefore that *no hysteresis loops were observed in the entirely c-oriented regions, whereas in the regions with (110)- and (100)-oriented grains the films exhibited saturated ferroelectric loops* with a remnant polarisation of 1 to $2\,\mu C/cm^2$ and a coercive field between 20 kV/cm and 60 kV/cm depending on the materials. These observations clearly prove that the macroscopic polarisation strongly depends on the density of *non-c-oriented* crystallites, and also on the degree of orientation of these crystallites with respect to the crystallographic direction along which the spontaneous polarisation lies, viz for SBT most probably the *a* axis [23]. The optimisation of the film orientation, i.e. the exact crystallographic direction of the spontaneous polarisation in bismuth-layered perovkites as well as the growth of bismuth-layered perovskite films only possessing this optimal orientation or having a predominant volume fraction of it are under investigation. The dependence of both fatigue and retention of thin films of bismuth-layered materials on their crystallographic orientation is an issue of fundamental interest and has also a strong potential impact on their applications. Further investigations should be carried out in order to clarify these questions.

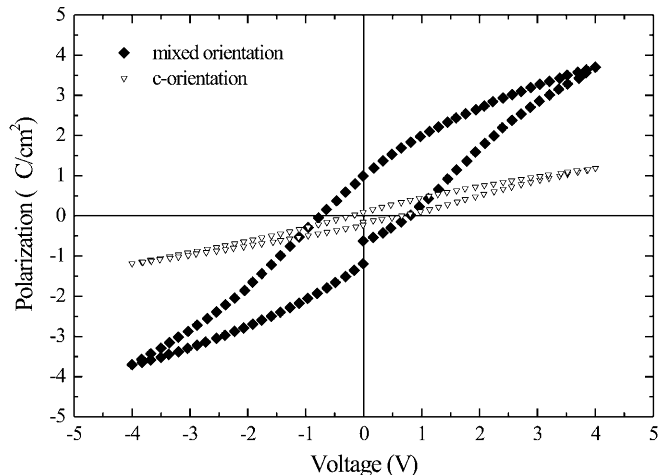

Fig. 5. Macroscopic ferroelectric hysteresis loop of an epitaxial SBT film on an epitaxial $LNO/CeO_2/YSZ/Si(100)$ hetereostructure, taken in a region with mixed orientation (high density of protruding epitaxial grains) and in a mostly *c*-oriented film, respectively

2.3.2 Domain switching and ferroelectric properties on the submicron scale. The sizes of the (110)- and (100)-oriented grains embedded in the *c*-oriented film matrix are of the order of 100 nm, well in the submicrometer range (Figs. 2 to 4). To date, only one method[3] is able to locally analyse the ferroelectric properties at this scale, and is able for instance to discriminate the ferroelectric properties of the grains from those of the matrix viz. *scanning force microscopy (SFM) in the piezoresponse mode* [44–47]. Harnagea et al. have refined the method in order to be able to extract quantitative information with a resolution of some tens of nm [36]. Only the component of the polarisation normal to the electrodes was investigated, which is the most common use of piezoresponses SFM.

[3] On extremely flat surfaces the changes in electrostatic force induced by the spontaneous polarisation could be recorded, in the so-called resonance method [42, 43]. This method is extremely sensitive to the electric fringing fields, as for instance the one produced by edges of three-dimensional structures. Therefore, and to the best of our knowledge, the piezoreponse SFM is the only method to be used on rough or structured surfaces.

Although the detection of the in-plane components of the polarisation is also possible, yet more complicated, it will not be discussed here. In the case of bismuth-layered perovskite materials only 180° domains have been reported and this limitation is therefore not a major concern. Figure 6a,b shows a topographic image $4 \times 4\ \mu m$ in area and the simultaneously acquired piezoresponse image of a region of the epitaxial SBT film of Figs. 2 and 3b. The piezoresponse image reveals the ferroelectric initial domain structure of this region of the film. The phase and offset voltage of the lock-in amplifier were adjusted so that positive polarisation appears in white and negative polarisation appears in black. A positive polarisation corresponds to a polarisation vector pointing up, towards the top electrode (in our case the conductive SFM tip) whereas a negative polarisation corresponds to a polarisation vector pointing down, towards the bottom LNO electrode and substrate. A grey colour indicates a piezoresponse at or below the detection limit and is therefore ascribed to a zero polarisation.

A striking feature of the piezoresponse image of Fig. 6b is that only the protruding grains give a net piezoresponse signal. The flat *c*-oriented background is uniformly grey, i.e. does not exhibit a normal polarisation. The protruding grains, in contrast, exhibit a very strong and well-contrasted piezoresponse (white or black, with few intermediate grey levels), demonstrating a measurable spontaneous polarisation normal to the film surface. In full accordance with the results of the macroscopic ferroelectric measurements presented above, these results demonstrate that *no polarisation is observed in the flat entirely c-axis-oriented regions, whereas in the regions with (110)- and (100)-axis oriented protruding grains the films exhibit a piezoresponse induced by their ferroelectric spontaneous polarisation*. These results are valid on the scale of the individual (110)- and (100)-oriented grains which are about 100 nm in size.

Tabata et al. grew natural and "artificial" bismuth-layered perovskites using a layer-by-layer deposition technique in order to control both the composition and the number of the perovskite blocks between two Bi_2O_2 layers [32, 33]. They obtained bismuth-layered perovskite films having compositions occurring in nature (they call it "natural" bismuth-layered perovskites) as well as compositions that are not occurring in nature (they call it "artificial" bismuth-layered perovskites), and showed that the films with an even Aurivillius parameter n exhibited no ferroelectricity along their crystallographic axis normal to the Bi_2O_2 layers, whereas films with an odd number n showed a spontaneous polarisation along this axis. It has to be noted that in their work, even the "natural" films were grown by extremely well-controlled layer-by-layer growth. Unlike Tabata et al. who showed it for engineered layers, we demonstrated here that this result is true also for bismuth-layered perovskite films epitaxially grown by PLD from stoichiometric ceramic targets, i.e. without any engineering of the structure of the films.

Figure 6c represents a higher magnification topographic image of a $1\ \mu m \times 1\ \mu m$ region, and the corresponding piezoresponse image (Fig. 6d) shows the initial domain structure of the single $350\ nm \times 250\ nm$ (100)-oriented SBT grain

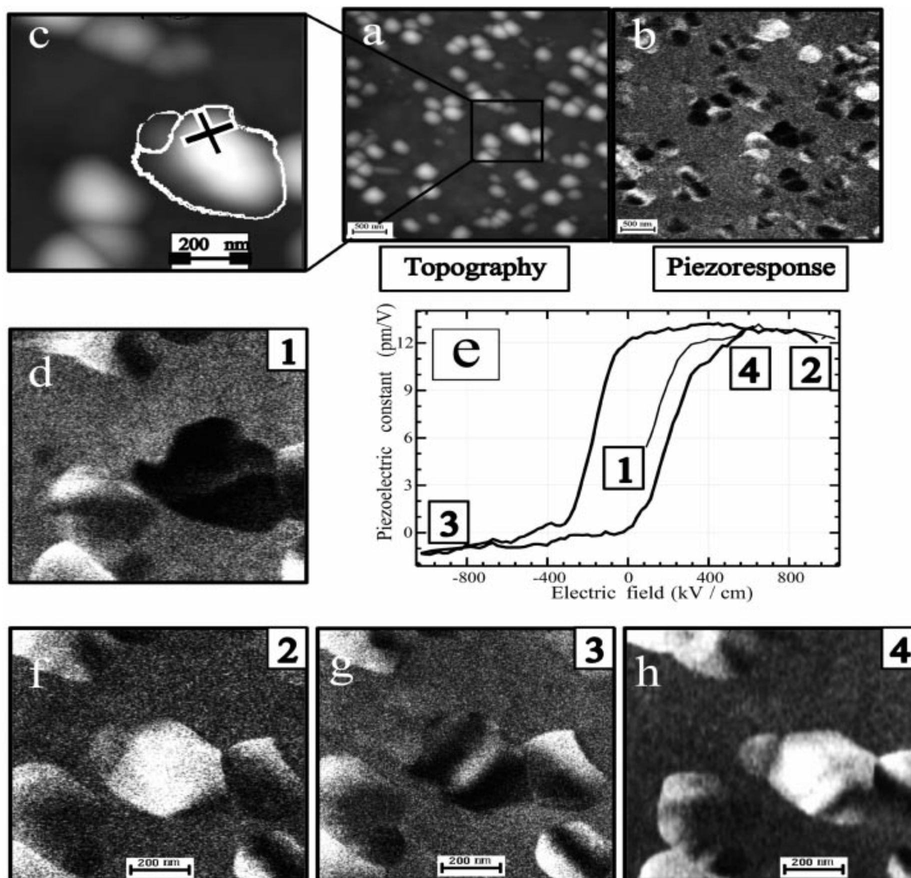

Fig. 6. Hysteresis loop of a $400\ nm \times 250\ nm$ (100)-oriented crystallite of SBT. The image shows simultaneously acquired topographic (*top-middle*) and piezoresponse (*top-right*) images of a $4 \times 4\ \mu m^2$ area of the sample. A higher magnification $1\ \mu m \times 1\ \mu m$ topographic image (*top-left*) as the corresponding piezoresponse images (1 to 4) show the domain structure of the crystallite before (1) and at various stages (2 to 4) of the local hysteresis loop taken at the place marked with a cross in the *top-left* topographic image. The different stages at which the piezoresponse images were taken are also indicated on the hysteresis loop

marked with a cross in Fig. 6c. The whole grain was in a negative polarisation state. The conductive tip was then located exactly at the point marked by the cross in Fig. 6c and a sequence of dc-bias voltage pulses was applied in order to record a local remnant hysteresis loop as explained in the experimental section. The recording was paused in the points marked 1 to 4 in the hysteresis loop of Fig. 6e, and piezoresponse images revealing the domain structure of the same region as that of Fig. 6c,d were acquired. Figure 6f shows for instance that after applying a voltage pulse of $+12$ V the entire grain which had a negative polarisation in Fig. 6d became positive. Figures 6g,h show again the switching of the grain in the negative and positive state, for -12 V and $+12$ V, respectively. It has to be noted that such locally resolved piezoresponse images at the submicron scale have been obtained for epitaxial BiT and BBiT films as well, extending the present discussion to bismuth-layered perovskites with an Aurivillius parameter $n = 2$ to 4 [35, 36]. Moreover, for BiT ($n = 3$), the only bismuth-layered perovskite with odd Aurivillius parameter n in this study, a small but still measurable polarisation has been detected also in c-oriented regions [36], in full accordance with the early macroscopic determination of the polarisation component along the c axis of BiT by Aurivillius and Fang as well as by Cummins and Cross [11, 13].

It can therefore be seen that grains as small as 100 nm in size exhibit measurable spontaneous polarisation and that this polarisation can be *readily switched* by means of an external electric field. Moreover, a careful observation of Fig. 6g reveals that a domain structure can still be observed *within* the grain itself, meaning that a stable domain configuration with domains smaller than 100 nm can exist. Similar results have been reported for arrays of artificial structures of PZT 100×100 nm in size, extending the generality to other materials and nanostructures [48]. The significance of these results is far reaching and the experimental results reported here are a contribution to the study of the fundamental problem of the minimum size of a stable ferroelectric structure. As in the case of macroscopic polarisation, a nanoscale-level investigation of fatigue and retention remains to be performed. This would give very useful information on the local mechanisms responsible for fatigue and retention loss, such as local imprint, domain pinning, etc.

3 Conclusions

Epitaxial thin films of three different Aurivillius-type compounds, viz $SrBi_2Ta_2O_9$ (SBT,x $n = 2$), $Bi_4Ti_3O_{12}$ (BiT, $n = 3$), and $BaBi_4Ti_4O_{15}$ (BBiT, $n = 4$) with good thickness and composition uniformity were grown on (100)-oriented epitaxial LNO electrodes on single-crystalline STO or on top of suitable epitaxial buffer layers on single-crystalline silicon. A comparative study of crystal orientation and orientation-dependent ferroelectric properties of these well-oriented BiT, SBT, and BBiT thin films was performed. Structure and morphology of the films were studied by XRD, SEM, SFM, and plan-view and cross-sectional TEM and these methods gave a set of independent and fully consistent results. It was shown that the morphology and microstructure of our films was not uniform. The films consisted of both fully c-oriented regions and of regions with mixed orientation. In the regions with mixed orientation the films were composed of two sublayers: the lower sublayer, growing on top of the epitaxial LNO electrode layer, was fully c-oriented whereas the upper layer consisted of (110)- and (100)-oriented grains embedded in a c-oriented matrix. The c-oriented matrix had a flat surface and the (110)- and (100)-oriented grains were protruding out of the matrix surface. The (110)- and (100)-oriented grains were single crystalline and had well-defined epitaxy relationships with the underlying layers and with the substrate.

The ferroelectric properties were determined both by macroscopic measurements and at the submicroscopic level by piezoresponse SFM. Saturated ferroelectric hysteresis loops were obtained for macroscopic regions with (110)- and (100)-oriented crystallites, whereas perfectly c axis oriented mascroscopic regions exhibited almost linear $P - E$ curves. The same behaviour was observed by piezoresponse SFM for SBT at the level of the individual protruding grains demonstrating that *only* the grains were responding, and therefore possess a spontaneous polarisation normal to the surface. These results were the same for BiT, SBT, and BBiT, although for BiT a small component of the polarisation along the c axis has also been evidenced. These significant results show that the ferroelectric properties in bismuth-layer-structured ferroelectric oxides for SBT and BBiT with an even Aurivillius parameter n ($n = 2$, 4) are *solely* due to (110)- and (100)-oriented grains, and that they are as well *strongly* or *mostly* governed by the non-c-oriented grains in BiT (odd Aurivillius parameter n). As the macroscopic ferroelectric properties of these layer-structured oxide thin films strongly depend on the crystalline orientation of the films, it is desirable indeed to grow fully a- or b-axis-oriented epitaxial films of bismuth-layer-structured ferroelectric perovskites.

This study also delivered convincing evidence that ferroelectricity still exists in structures with sizes as small as 100 nm, and that polarisation can be readily switched by means of an external electric field. Moreover, evidence was provided that even in single-crystalline grains about 100 nm in size a stable domain structure exists, with domain sizes of the order of magnitude of 20 to 30 nm. These results have a large significance both in addressing the fundamental problem of size-effects in ferroelectrics and also with respect to applications of ferroelectric thin films in high-density FeRAM memories. Further investigations on fatigue and retention both at the macroscopic and submicron level following the methodology of this work should now be performed.

Acknowledgements. The authors would like to thank Dr. S. Senz for his invaluable help in the X-ray texture analysis and to express their appreciation to Dr. N.D. Zakharov for many useful discussions regarding cross-section electron microscopy sample preparation. The RBS measurements were performed by Dr. R. Mattheis (IPHT, Jena) at the University of Jena. The authors also thankfully acknowledge the valuable technical contributions of Ms. S. Reichelt and of Mrs. D. Wild.

References

1. J.F. Scott: Ferroelectr. Rev. **1**, 1 (1998)
2. O. Auciello, J.F. Scott, R. Ramesh: Phys. Today **51**, 22 (1998)
3. D. Damjanovic: Rep. Prog. Phys. **61**, 1267 (1998)
4. J.F. Scott, C.A. Paz de Araujo: Science **246**, 1400 (1989)
5. Symetrix Corp.: Int. Patent H01L27/115, 21/320529/92 (1992)
6. R. Ramesh, A. Inam, W.K. Chan, B. Wilkens, K. Myers, K. Remschnig, D.L. Hart, J.M. Tarascon: Science **252**, 944 (1991)
7. C.A. Paz de Araujo, J.D. Cuchiaro, L.D. McMillan, M.C. Scott, J.F. Scott: Nature **374**, 627 (1995)

8. I.K. Yoo, S.B. Desu: J. Intell. Mater. Syst. Struct. **4**, 490 (1993)
9. A. Gruverman, O. Auciello, H. Tokumoto: Appl. Phys. Lett. **69**, 3191 (1996)
10. B. Aurivillius: Arkiv Kemi **2**(37), 519 (1950); E.C. Subba Rao: J. Am. Ceram. Soc. **45**, 166 (1962)
11. B. Aurivillius, P.H. Fang: Phys. Rev. **126**, 893 (1962); P.H. Fang, C.R. Robbins, B. Aurivillius: Phys. Rev. **126**, 892 (1962)
12. E.C. Subbarao: J. Phys. Chem. Solids **23**, 665 (1962)
13. S.E. Cummins, L.E. Cross: Appl. Phys. Lett. **10**, 14 (1967)
14. R.E. Newnham, R.W. Wolfe, J.F. Dorrian: Mat. Res. Bull. **6**, 1029 (1971)
15. T. Atsuki, N. Soyama, T. Yonezawa, K. Ogi: Jpn. J. Appl. Phys. **34**(1), 5096 (1995)
16. M. Tachiki, K. Yamamuro, T. Kobayashi: Mater. Sci. Eng. B **41**, 131 (1996)
17. T.-C. Chen, T. Li, X. Zhang, S.B. Desu: J. Mater. Res. **12**, 1569 (1997)
18. K. Watanabe, A.J. Hartmann, R. Lamb, J.F. Scott: J. Appl. Phys. **84**, 2170 (1998)
19. K. Takemura, T. Noguchi, T. Hase, Y. Miyasaka: Appl. Phys. Lett. **73**, 1649 (1998)
20. N.-J. Seong, C.-H. Yang, W.-C. Shin, S.-G. Yoon: Appl. Phys. Lett. **72**, 1374 (1998)
21. J. Lettieri, Y. Jia, M. Urbanik, C.I. Weber, J.-P. Maria, D.G. Schlom, H. Li, R. Ramesh, R. Uecker, P. Reiche: Appl. Phys. Lett. **73**, 2923 (1998)
22. A. Gruverman, Y. Ikeda: Jpn. J. Appl. Phys. **37**(2), L939 (1998)
23. Y. Shimakawa, Y. Kubo, Y. Nakagawa, T. Kamiyama, H. Asano, F. Izumi: Appl. Phys. Lett. **74**, 1904 (1999)
24. K.M. Satyalakshmi, M. Alexe, A. Pignolet, N.D. Zakharov, C. Harnagea, S. Senz, D. Hesse: Appl. Phys. Lett. **74**, 603 (1999)
25. B.H. Park, S.J. Huyn, S.D. Bu, T.W. Noh, J. Lee, H.-D. Kim, T.H. Kim, W. Jo: Appl. Phys. Lett. **74**, 1907 (1999)
26. A. Pignolet, M. Alexe, K.M. Satyalakshmi, S. Senz, D. Hesse, U. Gösele: Ferroelectrics (Proc. ECAPD IV, August 24–27, 1998, Montreux, Switzerland) **225**, 201 (1999)
27. A. Pignolet, C. Curran, M. Alexe, N.D. Zakharov, D. Hesse, U. Gösele: Integr. Ferroelectr. **21**, 485 (1998)
28. A. Pignolet, K.M. Satyalakshmi, M. Alexe, N.D. Zakharov, C. Harnagea, S. Senz, D. Hesse, U. Gösele: Proc. 11th Symposium on Integrated Ferroelectrics (ISIF99), March 7–10, 1999, Colorado Springs, USA
29. G.J. Willems, D.J. Wouters, H.E. Maes, R. Nouwen: Integr. Ferroelectr. **15**, 19 (1997)
30. S.K. Kim, M. Miyayama, H. Yanagida: J. Ceram. Soc. Jpn. **102**, 722 (1994)
31. E.C. Subbarao: Phys. Rev. **122**, 804 (1961)
32. H. Tabata, M. Hamada, T. Kawai: Mater. Res. Soc. Symp. Proc. **401**, 73 (1996)
33. H. Tabata, T. Yanagita, T. Kawai: IEICE Trans. Electron. **E81-C**, 566 (1998)
34. K.M. Satyalakshmi, R.M. Mallya, K.V. Ramanathan, X.D. Wu, B. Brainard, D.C. Gautier, N.Y. Vasanthacharya, M.S. Hegde: Appl. Phys. Lett. **62**, 1233 (1993)
35. C. Harnagea, M. Alexe, A. Pignolet, K.M. Satyalakshmi, D. Hesse, U. Gösele: Proceedings of the NATO Advanced Research Worlshop "Piezoelectric Materials: Advances in Science, Technology and Applications", May 24–27 1999 Predeal, Romania
36. C. Harnagea, A. Pignolet, M. Alexe, D. Hesse, U. Gösele: Appl. Phys. A, DOI 10.1007/s003390000177
37. C. Curran, S. Senz, A. Pignolet, M. Alexe, S. Welke, D. Hesse: Mater. Res. Soc. Symp. Proc. **474**, 15 (1997)
38. K.V.R. Prasad, K.B.R. Varma, A.R. Raju, K.M. Satyalakshmi, R.M. Mallya, M.S. Hegde: Appl. Phys. Lett. **63**, 1898 (1993)
39. K. Franke, J. Besold, W. Haessler, C. Seegebarth: Surf. Sci. Lett. **301**, L283 (1994)
40. A. Gruverman, O. Auciello, H. Tokumoto: Integr. Ferroelectr. **19**, 49 (1998)
41. S.B. Desu, D.P. Vijay, X. Zhang, B.P. He: Appl. Phys. Lett. **69**, 1719 (1996)
42. R. Lüthi, H. Haefke, K.-P. Meyer, E. Meyer, L. Howald, H.-J. Güntherrodt: J. Appl. Phys. **74**, 7461 (1993)
43. C.-H. Ahn, T. Tybell, L. Antognazza, K. Char, R.H. Hammond, M.R. Beasley, Ø. Fischer, J.-M. Triscone: Science **276**, 1100 (1997)
44. O. Auciello, A. Gruverman, H. Tokumoto, S.A. Prakash, S. Aggarwal, R. Ramesh: MRS Bulletin **23**, 33 (1998)
45. A. Gruverman, O. Auciello, H. Tokumoto: Appl. Phys. Lett. **69**, 3191 (1996)
46. A. Gruverman, H. Tokumoto, S.A. Prnakash, S. Aggarwal, B. Yang, M. Wuttig, O. Auciello, R. Ramesh, T. Venkantesan: Appl. Phys. Lett. **71**, 3492 (1997)
47. A. Gruverman, Y. Ikeda: Jpn. J. Appl. Phys. **37**, L939 (1998)
48. M. Alexe, C. Harnagea, W. Erfurth, D. Hesse, U. Gösele: Appl. Phys. A, DOI 10.1007/s003390000177